Aust. J. Phys., 1996, **49**, 745–64

Introduction to Light Forces, Atom Cooling, and Atom Trapping*

Craig Savage

Department of Physics, Faculty of Science,
Australian National University,
Canberra, ACT 0200, Australia.
email: Craig.Savage@anu.edu.au

Abstract

This paper introduces and reviews light forces, atom cooling, and atom trapping. The emphasis is on the physics of the basic processes. In discussing conservative forces the semiclassical dressed states are used rather than the usual quantised-field dressed states.

1. Forces

The idea that light exerts mechanical forces on matter arose early in astronomy. In 1619 Kepler suggested that it was the pressure of sunlight that made comet tails stream away from the Sun (Minogin and Letokhov 1987). And he was right. Nearly 250 years later Maxwell's theory of electromagnetism quantified light pressure. The light force on individual atoms was observed by Frisch, of Meitner and Frisch fission fame, in 1933. On Earth lasers provide the intensities necessary for exerting useful light forces. In the early 1970s Arthur Ashkin at Bell Labs accelerated, levitated and trapped micron-sized plastic spheres (Ashkin 1972). This work has developed into optical tweezers for manipulating small objects.

Today atoms are routinely cooled and trapped. Light-based mirrors, beamsplitters and lenses for atoms have been demonstrated (Adams *et al.* 1994*a*). These are the subject matter of atom optics, in which atomic de Broglie waves are manipulated as in classical optics. Atomic interferometers constructed with atom optics have extraordinary sensitivity (Adams *et al.* 1994*b*). Promising applications include atomic clocks, lithography, optical tweezers, and atom lasers or bosers (Wiseman and Collett 1995).

In this section we introduce the absorptive and dispersive limits of light forces. Absorptive forces are dissipative, and hence useful for cooling, while purely dispersive forces are conservative and hence useful for maintaining coherence. Section 2 deals with cooling, the first step towards trapping. Cooling has two important milestones: the Doppler limit and the recoil limit. At each 'limit' a new approach to cooling must be adopted. At present there appears to be no fundamental lower limit to the temperatures which can be achieved. Section 3

* Refereed paper based on a series of lectures presented to the Atom Optics Workshop, held at the Institute for Theoretical Physics, University of Adelaide, in September 1995.

0004-9506/96/040745$10.00

surveys methods for trapping ions and atoms. For neutral atoms we survey three basic approaches: dissipative traps, conservative traps and magnetic traps.

(1a) Classical Electrodynamics

The electric field of an electromagnetic wave sets a charged particle oscillating. The Lorentz interaction with the wave's magnetic field then pushes the charge in the direction of wave propagation. Since the wave gives momentum to the charge, it must itself have momentum. Relativistically, the presence of energy and momentum in the energy–momentum 4-vector means that field energy in some frame is momentum in another frame.

A recent experiment at the University of Queensland demonstrated the transfer of field angular momentum to micron-sized particles (He *et al.* 1995). The experiment was interesting because it was electromagnetic orbital angular momentum rather than photon spin that was transferred (Allen *et al.* 1992).

The field's intensity I ($\mathrm{W\,cm^{-2}}$) is given by the modulus of the Poynting vector $\boldsymbol{P} = c^2\ \epsilon_0 \boldsymbol{E} \times \boldsymbol{B}$. Using $p = E/c^2$ to convert this to a momentum flux gives the radiation pressure ($\mathrm{N\,m^{-2}}$):

$$\boldsymbol{R} = c\epsilon_0 \boldsymbol{E} \times \boldsymbol{B}, \quad |\boldsymbol{R}| = I/c\,. \tag{1}$$

The major macroscopic application of this force may well turn out to be solar sailing (Mallove and Matloff 1989). The solar flux at the Earth's orbit is about 1400 $\mathrm{W\,m^{-2}}$, corresponding to a pressure of $4{\cdot}7\ \mu\mathrm{N\,m^{-2}}$. Perfect reflection doubles this pressure. Aluminium-coated mylar films a few microns thick have densities of around $5\ \mathrm{g\,m^{-2}}$ giving a payload, free acceleration of around $2\ \mathrm{mm\,s^{-2}}$. This is enough for interplanetary travel, taking about a year to reach Mars.

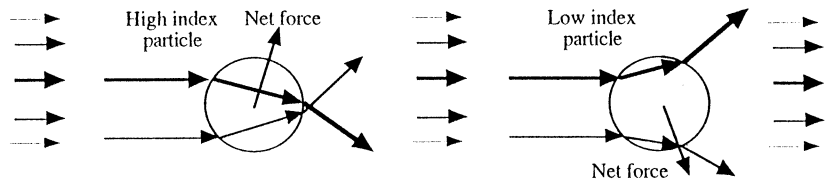

Fig. 1. Optical ray diagrams showing the origin of dispersive forces on transparent macroscopic particles. The arrows represent light rays with thickness proportional to intensity. The columns of arrows represent the light beam. The left- and right-hand circles respectively represent particles with refractive index higher and lower than that of the surroundings. Since the light has momentum and changes direction by refraction, momentum is transferred to the particles. The net momentum transfer is determined by the most intense rays, closest to the beam centre.

The most useful macroscopic light force today is the dispersive force used in optical tweezers. An object with higher refractive index than its surroundings is attracted towards high-field regions, while one with lower index is repelled. This can be understood by considering the momentum changes of light rays refracted through the particles, as shown in Fig. 1. In Section 1*c* we shall derive the corresponding results for atoms. A field detuned above resonance, which induces a refractive index $n < 1$, repels atoms from high-field regions, while a below-resonance field, which induces a refractive index $n > 1$, attracts atoms (Loudon 1973).

Fortunately most biological objects have a greater refractive index than water and so can be stably manipulated with the waist of a laser beam. Ashkin *et al.* (1987) showed that live viruses and bacteria could be manipulated with microscope-based infrared optical tweezers. The list of biophysical applications to date includes manipulation of single DNA molecules (Chu 1991) and of human gametes (Tadir *et al.* 1991), cell micro-surgery (Steubing *et al.* 1991), and studies of motor proteins (Ashkin *et al.* 1990) and mitotic chromosomes (Liang *et al.* 1991).

(1b) Dissipative Forces

Quantising the field with plane-wave spatial modes $\exp(i\boldsymbol{k}.\boldsymbol{r})$ gives field quanta, called photons, with momentum $\hbar\boldsymbol{k}$. The dissipative, or scattering, force is then particularly simple to understand. Each photon absorption gives a momentum kick $\hbar\boldsymbol{k}$ to the absorber. Each subsequent spontaneous emission gives a kick of the same magnitude but in a random direction, producing no average force. However the resultant momentum fluctuations are what limit cooling, as we shall see in Section 2*a*.

The dissipative force from a laser can slow a counter-propagating beam of atoms. The changing Doppler shift as the atoms slow can be overcome by chirping the laser frequency or by Zeeman-shifting the atomic transition frequency with a spatially varying magnetic field. A slowed beam may be transversely cooled by two-dimensional optical molasses. This consists of two lasers counter-propagating transversely to the atomic beam and tuned below resonance—so-called red detuning. Transverse motion Doppler-shifts the counter-propagating beam towards resonance and the co-propagating beam away from resonance. Hence more counter-propagating photons are absorbed and the atom slows. This process is called Doppler cooling.

There is a limit to the temperature achievable by Doppler cooling—the so-called Doppler limit,

$$k_{\mathrm{B}}T_{\mathrm{Dop}} = \frac{\hbar\gamma}{2}, \qquad \text{Doppler limit}, \tag{2}$$

where γ is the transition linewidth or inverse lifetime. Note that here and hereafter we use 'temperature' in a conventional sense to denote the mean energy without implying thermal equilibrium. For the D line of Na, $T_{\mathrm{Dop}} \approx 240\ \mu\mathrm{K}$. The Doppler limit is interesting because it depends only on the linewidth. The molasses cools the atoms until their kinetic energy equals half the transition energy uncertainty $\hbar\gamma$ (Stenholm 1986). This is reasonable since the atoms are inelastically scattering photons. Scattered photons will typically differ in energy by the linewidth. The difference between the scattered photon energy and the absorbed photon energy appears as the atomic kinetic energy. In Section 2*a* we derive the Doppler limit by balancing the cooling rate with the heating rate due to the spontaneous emission recoils.

(1c) Conservative Forces and Semiclassical Dressed States

Forces arise when there is a spatial gradient in the expectation value of a system's energy, i.e. its Hamiltonian. A two-level atom interacting with the electric field $\boldsymbol{E}(\boldsymbol{r},t)$ has the Hamiltonian (Allen and Eberly 1987)

$$H = \hbar(\omega_A/2)(|e\rangle\langle e| - |g\rangle\langle g|) - \boldsymbol{d}\cdot\boldsymbol{E}(\boldsymbol{r},t), \tag{3}$$

where $|g\rangle$ and $|e\rangle$ are the ground and excited atomic states respectively, $\hbar\omega_A$ is the transition energy, and $\boldsymbol{d}$ its electric dipole moment operator. Assuming no spatial dependence of ω_A, the Heisenberg equation of motion for the momentum $\boldsymbol{p}$ is

$$\boldsymbol{F} = \frac{d\boldsymbol{p}}{dt} = \frac{1}{i\hbar}[\boldsymbol{p}, H] = -\nabla H = \nabla(\boldsymbol{d}\,.\,\boldsymbol{E}(\boldsymbol{r},t))\,, \tag{4}$$

since the time derivative of the momentum is the force $\boldsymbol{F}$. Forces arising from a gradient in the Hamiltonian are conservative, and there is no energy dissipation as in Doppler cooling. The force described by equation (4) is known as the gradient force or dipole force.

The eigenstates of the Hamiltonian, equation (3), are called dressed states (Cohen-Tannoudji *et al.* 1992). The energy expectation value is the sum over the dressed states of the product of their energies and populations. Dipole forces arise due to gradients in the dressed state energies, or due to dressed state population gradients, or both.

In this paper we only consider the semiclassical case in which $\boldsymbol{E}(\boldsymbol{r},t) = \boldsymbol{\mathcal{E}}(\boldsymbol{r})\exp(-i\omega t) + \boldsymbol{\mathcal{E}}^*(\boldsymbol{r})\exp(i\omega t)$ is a classical field. Ignoring the kinetic energy and making the rotating wave approximation, the Hamiltonian becomes

$$\begin{aligned} H_{SC} &= \hbar(\omega_A/2)(|e\rangle\langle e| - |g\rangle\langle g|) \\ &\quad - id\left(|e\rangle\langle g|\mathcal{E}(\boldsymbol{r})e^{-i\omega_L t} - |g\rangle\langle e|\mathcal{E}^*(\boldsymbol{r})e^{i\omega_L t}\right)\,, \end{aligned} \tag{5}$$

where ω_L is the field frequency and d is the dipole matrix element related to the transition linewidth by $\gamma = 4\omega_A^3 d^2/3\hbar c^3$. We eliminate the time dependence of the field by working in the interaction picture with $H_0 = \hbar(\omega_L/2)(|e\rangle\langle e| - |g\rangle\langle g|)$ and with the interaction Hamiltonian

$$\begin{aligned} H_{SC,I} = &-\hbar(\Delta/2)(|e\rangle\langle e| - |g\rangle\langle g|) \\ &- id(|e\rangle\langle g|\mathcal{E}(\boldsymbol{r}) - |g\rangle\langle e|\mathcal{E}^*(\boldsymbol{r}))\,, \end{aligned} \tag{6}$$

where we have defined the field–atom detuning as $\Delta \equiv \omega_L - \omega_A$. The semiclassical dressed states are the eigenstates of this Hamiltonian. They and their energies are

$$|1\rangle \equiv \cos(\theta)|g\rangle + i\sin(\theta)|e\rangle, \quad E_1 = -\frac{\hbar}{2}\mathcal{R}; \tag{7}$$

$$|2\rangle \equiv \sin(\theta)|g\rangle - i\cos(\theta)|e\rangle, \quad E_2 = +\frac{\hbar}{2}\mathcal{R}; \tag{8}$$

$$\cos(2\theta) \equiv -\Delta/\mathcal{R}, \quad \sin(2\theta) \equiv \Omega/\mathcal{R}\,. \tag{9}$$

We have introduced the Rabi frequency and the generalised Rabi frequency

$$\Omega \equiv 2d|\mathcal{E}|/\hbar, \qquad \text{Rabi frequency}, \tag{10}$$

$$\mathcal{R} \equiv \sqrt{\Delta^2 + \Omega^2}, \quad \text{generalised Rabi frequency}. \tag{11}$$

The difference between the generalised Rabi frequency and the detuning is referred to as the light shift. It is the shift in the transition frequency due to interaction with the light field.

Consider a ground-state atom slowly moving into a laser beam. The adiabatic theorem (Messiah 1966) implies that it remains in the Hamiltonian eigenstate continuously connected to the zero-field ground state. Which dressed state this is depends on the field detuning:

$$\Delta > 0 \Rightarrow \cos 2\theta = -1 \Rightarrow \cos\theta = 0 \Rightarrow |2\rangle = |g\rangle\,; \tag{12}$$

$$\Delta < 0 \Rightarrow \cos 2\theta = 1 \Rightarrow \cos\theta = 1 \Rightarrow |1\rangle = |g\rangle\,. \tag{13}$$

Consequently the Hamiltonian expectation value is just the eigenvalue $\pm\hbar\mathcal{R}/2$. In the limit of detuning Δ large compared to the Rabi frequency Ω, we have

$$\langle H\rangle \approx \pm\frac{\hbar}{2}\mathcal{R} \approx \pm\frac{\hbar}{2}|\Delta|\left(1 + \tfrac{1}{2}\left(\frac{\Omega}{\Delta}\right)^2\right). \tag{14}$$

For constant detuning only the second term contributes to the gradient, corresponding to an effective potential

$$V(\boldsymbol{r}) = \tfrac{1}{4}\frac{\hbar\Omega^2}{\Delta}\,. \tag{15}$$

This is the mechanical potential produced by intensity gradients of a far-detuned field. It has the same sign as $\Delta = \omega_{\mathrm{L}} - \omega_{\mathrm{A}}$ so for $\Delta > 0$, blue detuning, it rises in high-intensity regions from which atoms are therefore repelled. Otherwise, for $\Delta < 0$, red detuning, atoms are attracted to high-intensity regions.

This far-detuned potential has a simple interpretation in terms of the bare atomic states. The excited-state population $P_{\mathrm{e}} \approx s/2$ is given by equation (19), and the atom is excited by absorbing photons with energy $\hbar\Delta$ greater than that of the excited atom. The energy excess $P_{\mathrm{e}}\hbar\Delta$ is exactly the potential, equation (15); the energy excess appears as mechanical potential energy.

The red-detuned dipole force can be used to construct an atom trap called the far off-resonance trap or FORT. It is essentially optical tweezers for atoms. A FORT trap has been demonstrated to operate at 65 nm detuning, confining Rb atoms at 0·4 mK (Miller *et al.* 1993).

Since it is non-dissipative, the dipole force is most suitable for constructing atom optics devices which preserve quantum coherence. This is a requirement for atom interferometry. Proposed atom waveguides constructed from hollow optical fibres utilise the dipole force to repel the atoms from the fibre walls (Marksteiner *et al.* 1994).

(1d) A Sense of Scale

Let's get an idea of the scale of the forces, masses, accelerations and so on that are typical of atom optics. For concreteness we consider a sodium atom which has a mass of $M = 23$ au $= 3{\cdot}8 \times 10^{-26}$ kg. The yellow D-line transition is $3S_{1/2} \leftrightarrow 3P_{3/2}$, with wavelength $589{\cdot}0$ nm and lifetime $16{\cdot}4$ ns (Adams *et al.* 1994*a*). A saturated sodium atom has 50% probability of being excited, so on average it absorbs and emits one photon every 33 ns or 3×10^7 photons s^{-1}. The impulse from the absorbed photon momenta is $I = (3 \times 10^7)\hbar k = 3{\cdot}4 \times 10^{-20}$ (kg m s^{-1}) s^{-1}. The corresponding acceleration of the atom is $I/M \approx 10^6$ m s^{-1} $\approx 10^5$ g. At this acceleration a 500 m s^{-1} atom is brought to rest in half a millisecond over about 13 cm.

The Doppler limit temperature, equation (2), of 240 μK corresponds to a thermal velocity

$$v_{\rm d} = \sqrt{\frac{\hbar\gamma}{4M}} = 30 \text{ cm s}^{-1}. \tag{16}$$

By comparison, at a temperature of 300 K the average thermal speed in a Maxwellian distribution is $\sqrt{8k_{\rm B}T/\pi M} \approx 530$ m s^{-1}.

The recoil speed from a photon emission or absorption is

$$v_{\rm r} = \frac{\hbar k}{M} = 3 \text{ cm s}^{-1}. \tag{17}$$

A thermal speed of 3 cm s^{-1} corresponds to a temperature of about 1 μK. This recoil limit speed will turn out to be the lower limit to speeds attainable by cooling mechanisms for which the cold atoms interact with light. Since $p = h/\lambda$ for both matter and light, the corresponding atomic de Broglie wavelength is, by momentum conservation, just that of the photon: $\lambda_{\rm dB} = \lambda_{\rm light} = 589$ nm. The corresponding kinetic energy is $Mv_{\rm r}^2/2 = 1{\cdot}7 \times 10^{-29}$ J. This is nearly 10 orders of magnitude smaller than the energy of a photon, $\hbar\omega = 3{\cdot}4 \times 10^{-19}$ J. It corresponds to a detuning of about $\Delta = 1{\cdot}7 \times 10^{-29}/\hbar = 1{\cdot}6 \times 10^5$ rad s^{-1}.

2. Cooling

A great variety of cooling methods have been demonstrated (Metcalf and van der Straten 1994). They can be classified with respect to two limits representing the lowest temperatures attainable with the particular method, the Doppler limit and the recoil limit:

$$T_{\rm Dop} = \frac{\hbar\gamma}{2k_{\rm B}}, \quad \text{Doppler limit}, \qquad T_{\rm recoil} = \frac{(\hbar k)^2}{2Mk_{\rm B}}, \quad \text{recoil limit}. \tag{18}$$

For Na these are respectively 240 μK and $1{\cdot}2$ μK. Cooling using Doppler tuning of an atomic transition is Doppler-limited due to heating by the scattered photon recoils. Sub-Doppler cooling utilises the multi-level nature of atoms to approach the recoil limit. It is limited by the fact that the coldest atoms have scattered a last photon and hence have at least the photon recoil energy. Sub-recoil cooling requires passive velocity groups for the atoms to accumulate in without scattering photons.

(2a) Doppler Cooling

Doppler cooling was introduced in Section 1*b*. In this section the Doppler cooling limit is derived by balancing the viscous cooling with the recoil heating. We assume a two-level atom with velocity $\boldsymbol{v}$ and transition frequency ω_A interacting with 1D optical molasses at frequency ω_L. The optical molasses consists of two counter-propagating laser beams: beam 1 with wavevector $\boldsymbol{k}$ and beam 2 with wavevector $-\boldsymbol{k}$. The field–atom detuning is denoted by $\Delta = \omega_L - \omega_A$. From the semiclassical Bloch equations (Allen and Eberly 1987) the steady-state excited state population is

$$P_e = \tfrac{1}{2}\frac{s}{1+s}, \qquad s \equiv \frac{\Omega^2/2}{(\Delta - \boldsymbol{k}\,.\,\boldsymbol{v})^2 + \gamma^2/4}, \tag{19}$$

where s is the saturation parameter, expressed in terms of the Rabi frequency Ω, equation (10), for the atom–field interaction.

We now assume that the transition is sufficiently far from saturation $s \ll 1$ that the absorption from each beam is independent. Then the force on the atom is the sum of the momentum absorption rate from each beam

$$\begin{aligned} F &\approx \hbar k \gamma P_{e,1} - \hbar k \gamma P_{e,2} \\ &\approx \hbar k \gamma \tfrac{1}{2}(s_1 - s_2), \quad s_i \ll 1\,. \end{aligned} \tag{20}$$

For the small velocities at the Doppler cooling limit we can expand s in $v = |\boldsymbol{k}\,.\,\boldsymbol{v}|/|\boldsymbol{k}|$ to get

$$s_{1/2} \approx s_0\left(1 \pm \frac{2\Delta k v}{\Delta^2 + \gamma^2/4}\right), \tag{21}$$

where s_0 is the zero-velocity saturation parameter. Substituting these expansions into the force equation (20) gives

$$F \approx \hbar k \gamma s_0 \frac{2\Delta k}{\Delta^2 + \gamma^2/4} v\,. \tag{22}$$

For red detuning, $\Delta < 0$, this is a viscous-type damping force proportional to the atomic velocity. The associated kinetic energy cooling rate is

$$\frac{\mathrm{d}\langle E_{\mathrm{cool}}\rangle}{\mathrm{d}t} = \langle Fv\rangle = \hbar k \gamma s_0 \frac{2\Delta k}{\Delta^2 + \gamma^2/4}\langle v^2\rangle\,, \tag{23}$$

where the angle brackets denote an average over the atomic ensemble. We next consider the photon recoil heating of the atom.

Each spontaneous emission kicks the atom in a random direction with momentum magnitude $\hbar k$, producing a random walk in momentum space. After N emissions the mean squared momentum magnitude is $\langle p^2\rangle = N(\hbar k)^2$. The total momentum diffusion rate is four times this. One factor of 2 comes from spontaneous emission

from the two beams. The other factor of 2 comes from the absorption, which is also a random process (Cohen-Tannoudji 1992). Using the spontaneous emission rate $\gamma s_0/2$, we then have the following expression for the kinetic energy heating rate:

$$\frac{\mathrm{d}\langle E_{\mathrm{heat}}\rangle}{\mathrm{d}t} = 4\frac{\mathrm{d}(\langle p^2\rangle/2M)}{\mathrm{d}t} \approx 4\frac{1}{2M}\gamma\frac{s_0}{2}(\hbar k)^2, \quad s_0 \ll 1\,, \tag{24}$$

where we have used the zero-velocity saturation parameter, as our goal is to find the temperature minimum. At equilibrium the sum of this heating rate and the cooling rate, equation (23), is zero:

$$\frac{\mathrm{d}\langle E_{\mathrm{cool}}\rangle}{\mathrm{d}t} + \frac{\mathrm{d}\langle E_{\mathrm{heat}}\rangle}{\mathrm{d}t} = 0 \quad \Rightarrow \quad \frac{2\Delta}{\Delta^2+\gamma^2/4}\langle v^2\rangle + \frac{\hbar}{M} = 0 \Rightarrow \tag{25}$$

$$\langle \tfrac{1}{2}Mv^2\rangle = -\frac{\hbar}{2}\frac{\Delta^2+\gamma^2/4}{2\Delta} = -\frac{\hbar\gamma}{8}\left(\frac{2\Delta}{\gamma}+\frac{\gamma}{2\Delta}\right). \tag{26}$$

The last bracketed expression has a minimum of -2 at $2\Delta/\gamma = -1 \Rightarrow \Delta = -2\gamma$, so this detuning gives the minimum mean kinetic energy. This defines the Doppler limit energy $k_{\mathrm{B}}T_{\mathrm{Dop}}/2$, so

$$T_{\mathrm{Dop}} = \frac{\hbar\gamma}{2k_{\mathrm{B}}}, \tag{27}$$

a result explained heuristically at the end of Section 1*b*.

(2b) Sisyphus Cooling

The Doppler cooling discussed in the previous section only works for light intensities below saturation. Above saturation stimulated processes become important and cooling only occurs for blue detuning! This blue cooling is stronger than Doppler cooling but does not achieve such low temperatures (Aspect *et al.* 1986). This is because although the damping is stronger so are the fluctuations.

It is an example of a more general mechanism called Sisyphus cooling, after the mythological Sisyphus, king of Corinth, who was doomed by Zeus to roll a rock uphill forever. In a standing wave the Rabi frequency Ω varies with the spatial mode function from zero at the nodes (zero field) to a maximum at the anti-nodes. Hence so does the energy splitting of the semiclassical dressed states $\hbar\mathcal{R}$, equation (11). Cooling occurs because, as we shall see, spontaneous emission is most likely to occur from energy maxima into energy minima. The atom then moves up the energy hill and is again most likely to emit at the maximum. On average, kinetic energy is converted to atom–field interaction energy which is lost by spontaneous emission.

A detailed explanation using dressed atomic states with a quantised field has been given by Dalibard and Cohen-Tannoudji (1985). By contrast, we use semiclassical dressed states, which were introduced in Section 1*c*. Any dressed state with an excited state component can spontaneously emit into any dressed

state with a ground state component. In general a dressed state can spontaneously emit into itself as well as into the other dressed state.

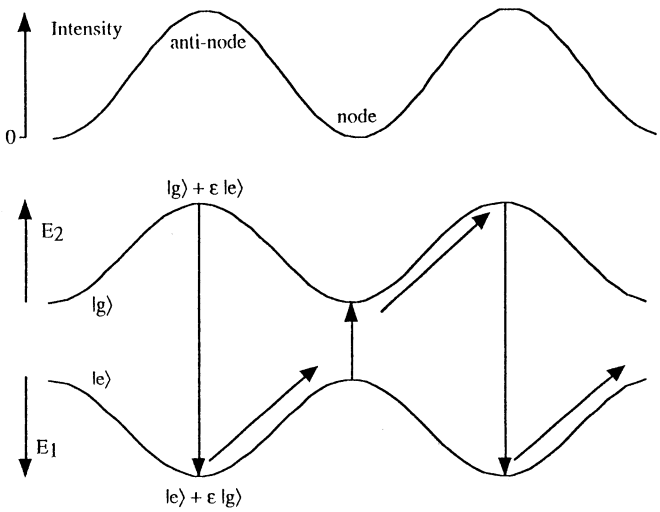

Fig. 2. Mechanism for blue Sisyphus cooling. The top curve is the standing-wave field intensity as a function of position. The lower two curves are the energies E_1 and E_2 of the dressed states $|1\rangle$ and $|2\rangle$. The vertical arrows denote spontaneous emissions, which are shown at their most probable locations. The diagonal arrows denote the atomic motion and ε is a number $\ll 1$.

We now explain blue Sisyphus cooling with reference to Fig. 2. In a standing-wave field the electric field is zero at the nodes and is a maximum at the anti-nodes. Hence the generalised Rabi frequency, equation (11), varies from $|\Delta|$ at the nodes to $\sqrt{\Delta^2+\Omega^2}$ at the anti-nodes. Here $|2\rangle$ is the higher-energy state and for blue detuning, $\Delta > 0$, it equals the ground state $|g\rangle$ at a node. It increases in energy and mixes in the excited state $|e\rangle$ as the field increases. Here $|1\rangle$ is the lower energy state and for blue detuning it equals $|e\rangle$ at the nodes; it decreases in energy and mixes in the ground state with increasing field. Consequently at anti-nodes $|2\rangle$ has its maximum energy and $|1\rangle$ its minimum energy, while at nodes the opposite holds. But $|2\rangle$ is most likely to spontaneously emit at anti-nodes since there it has the largest excited state component. It can decay either to itself, in which case only the photon energy $\hbar\omega_L$ is lost, or to $|1\rangle$, in which case the larger energy $\hbar(\omega_L + \mathcal{R})$ is lost. (Recall that the dressed states are defined in a picture rotating with frequency ω_L, so $\hbar\omega_L$ is the energy zero.) In contrast, the dressed state $|1\rangle$ is most likely to spontaneously emit at nodes, where it is exactly the bare excited state, $|e\rangle$. At a node it has no ground state component and hence can only decay to $|2\rangle$, losing energy $\hbar(\omega_L - \Delta)$. Since this is smaller than $\hbar(\omega_L + \mathcal{R})$ more energy than $\hbar\omega_L$ is lost on average per spontaneous emission. This energy cannot be provided by the photons absorbed from the field, which have energy $\hbar\omega_L$. It comes from kinetic energy and hence cools the atom.

The transfer of kinetic energy to atom–field interaction energy is the Sisyphus mechanism. An atom which has just spontaneously emitted is most likely to be

in the energy minimum for its dressed state. Any motion increases the atom–field interaction energy until it is most likely to spontaneously emit again at the top of the energy hill. Thus kinetic energy is transformed into interaction energy which is dissipated by spontaneous emission.

Consider a sequence of spontaneous emissions which start and end in the same dressed state while passing through the other dressed state. The most likely starting point is at an energy maximum and the most likely end point an energy minimum. Hence the total process of (at least) two spontaneous emissions dissipates the energy difference between the maximum and minimum, which is just the light shift. Sequences which increase the energy are possible, but less likely.

The limiting temperature is determined by the heating due to spontaneous emissions. Emission from $|2\rangle$ is most likely to leave the atom in $|2\rangle$ with no cooling effect, but recoil heating still occurs.

(2c) Spatially Dependent Optical Pumping

To cool below the Doppler limit, equation (27), requires multi-level atoms. Since atoms are multi-level and since theorists like two-level atoms it is perhaps not surprising that sub-Doppler cooling was discovered experimentally (Lett *et al.* 1988). A common feature of the various sub-Doppler, but super-recoil, cooling schemes is optical pumping.

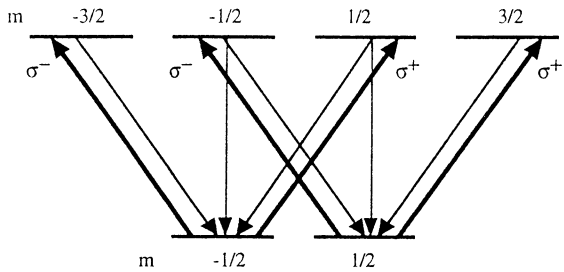

Fig. 3. Optical pumping in a $J = \frac{1}{2} \leftrightarrow J = \frac{3}{2}$ transition. States are labelled by their magnetic quantum number, m. The thick arrowed lines represent transitions induced by either σ^+ or σ^- polarised light. The thin single arrows represent spontaneous emission.

Optical pumping is the transfer of population between atomic magnetic sub-levels. For definiteness we consider a total angular momentum $J = \frac{1}{2} \leftrightarrow J = \frac{3}{2}$ transition, see Fig. 3. Circularly polarised light is either σ^+ or σ^- with photon angular momentum $+\hbar$ or $-\hbar$ respectively. An atom in the $m = -\frac{1}{2}$ ground state sub-level can be excited into the $m = +\frac{1}{2}$ excited state sub-level by absorbing a σ^+ photon, and into the $m = -\frac{3}{2}$ excited state sub-level by absorbing a σ^- photon. Similarly the $m = +\frac{1}{2}$ ground sub-level is excited into either the $m = +\frac{3}{2}$ or $m = -\frac{1}{2}$ excited sub-levels by absorbing a σ^+ or σ^- photon respectively. Absorption of σ^+ polarised light increases the magnetic quantum number m while absorption of σ^- polarised light decreases it. The net result of cycles of absorption and spontaneous emission in circularly polarised light is optical

pumping: the preferential population of ground sub-levels with extremal m; in this case either the $m = \frac{1}{2}$ or $m = -\frac{1}{2}$ sub-level. In the following we are only concerned with weak fields so that the excited state population is negligible.

Spatially dependent optical pumping occurs when the pumped sub-level depends on position. In 3D this is unavoidable and is usually achieved with three pairs of counter-propagating laser beams. Because the atoms are moving, the state of the atom lags behind the local steady state. Cooling is achieved when this lag is used to remove energy from the atoms as they are optically pumped towards local equilibrium. Since polarisation gradient cooling is one of the more effective of such mechanisms, we consider it next.

(2d) Polarisation Gradient Cooling

Polarisation gradient cooling uses counter-propagating beams with perpendicular linear polarisations to achieve spatially dependent optical pumping, see Fig. 4. This is known as the 'lin perp lin' configuration. Atoms lose kinetic energy by a Sisyphus mechanism in which the hills are due to light shifts. 3D lin $\perp$ lin cooling to within a few recoil velocities, about 25 μK for Na, has been achieved (Cohen-Tannoudji and Phillips 1990).

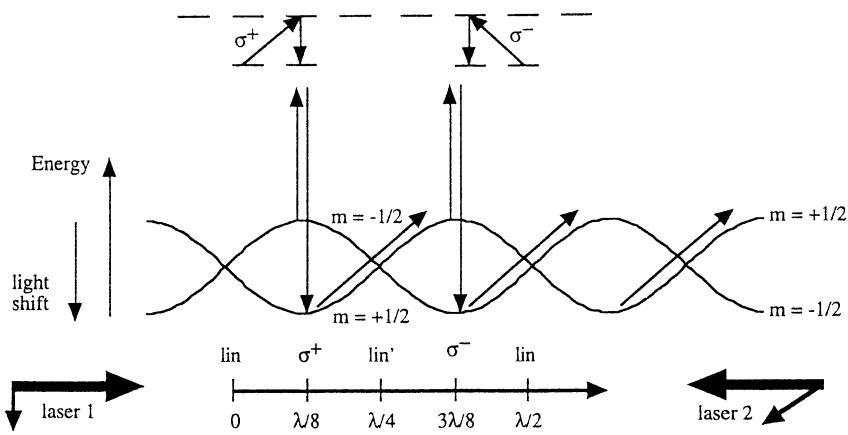

Fig. 4. Mechanism for polarisation gradient lin $\perp$ lin cooling. A $J = \frac{1}{2}$ ground level, as shown in Fig. 3, is assumed. The top atomic energy level diagrams indicate the local direction of optical pumping. The curves show the energies of the dressed ground sub-levels for red-detuned light. The pairs of vertical arrows show optical pumping at the positions where it is most probable. The horizontal axis shows how the polarisation of the field varies over half a wavelength due to the perpendicularly polarised counter-propagating lasers.

The polarisation varies with a period of $\lambda/2$ from linear to σ^+, to the orthogonal linear, to σ^-, and back to linear, see Fig. 4. The linear polarisation is at angle $\pi/4$ to the input linear polarisations. This can be seen from the expression for the electric field in the lin $\perp$ lin configuration,

$$\boldsymbol{E} = \boldsymbol{x}\sin(kz - \omega t) + \boldsymbol{y}\sin(kz + \omega t)\,, \tag{28}$$

where $\boldsymbol{x}$ and $\boldsymbol{y}$ are unit vectors in the x and y directions. Using $k = 2\pi/\lambda$ and some trigonometric identities gives

$$\boldsymbol{E} = (\boldsymbol{y} - \boldsymbol{x})\cos(2\pi z/\lambda)\sin(\omega t) + (\boldsymbol{x} + \boldsymbol{y})\sin(2\pi z/\lambda)\cos(\omega t)\,. \tag{29}$$

At $z = 0$ the field is linearly polarised in the $\boldsymbol{y} - \boldsymbol{x}$ direction. At $z = \lambda/8$, $\sin(2\pi z/\lambda) = \cos(2\pi z/\lambda) = 1/\sqrt{2}$ and the magnitude of the field is constant in time and hence it is circularly polarised. At $z = \lambda/4$, $\sin(2\pi z/\lambda) = 1$ and the field is linearly polarised in the $\boldsymbol{x} + \boldsymbol{y}$ direction. At $z = 3\lambda/8$, $\sin(2\pi z/\lambda) = 1/\sqrt{2}$ and $\cos(2\pi z/\lambda) = -1/\sqrt{2}$, and the field is again circularly polarised, but this time with the opposite rotation sense. This polarisation gradient produces spatially dependent optical pumping.

Lin $\perp$ lin cooling uses light shifting of the ground sub-levels. Light shifting was discussed for two-level transitions in Section 1*c*. The total shift of the $m = \pm\frac{1}{2}$ sub-levels is the sum of the shifts due to each of the two transitions to which they are coupled by the lasers. The proportion of σ^- and σ^+ varies spatially, and since each transition has a different coupling strength, as determined by the Clebsch–Gordon coefficients, the light shifts of the ground sub-levels depend on position.

These shifts are negative for red detuning and for the $m = -\frac{1}{2}$ sub-level are maximum in magnitude where the field is σ^- polarised, and minimum where it is σ^+. The opposite is true for the $m = +\frac{1}{2}$ sub-level, Fig. 4. At the minimum light shift positions, optical pumping into the other sub-level is strongest. The result is that atoms move uphill until they are optically pumped into the other sub-level.

This pumping takes energy out of the atom provided that the atomic state lags the local equilibrium by somewhat less than the optical pumping time τ_p. This is the average time for optical pumping to transfer population between the ground sub-levels and is proportional to the intensity. Hence lin $\perp$ lin cooling works best for velocities v_ideal such that the atom travels $\lambda/4$ in τ_p, $v_\mathrm{ideal} \approx \lambda/(4\tau_\mathrm{p})$. Atoms which are moving too fast do not respond to the local pumping and hence do not lose energy. Atoms which are moving too slowly are pumped to the other sub-level before reaching the top of the hill and hence lose less energy.

Polarisation gradient cooling does not achieve the recoil limit. Cooling closer to the recoil limit can be achieved after trapping the atoms in an optical lattice. Adiabatically expanding the lattice cools the atoms. Reduction of the Cs temperature from the 3 μK achievable with polarisation gradient cooling to $0{\cdot}7\ \mu$K has been demonstrated with adiabatic cooling (Kastberg *et al.* 1995). This is short of the Cs recoil limit of $0{\cdot}13\ \mu$K.

Velocity-selective Coherent Population Trapping (VSCPT)

For cooling below the recoil limit the problem is to avoid having the recoil from the last photon emitted determine the temperature. There are two successful approaches: momentum diffusion into a passive zero-velocity group, and evaporation of the hottest atoms, avoiding photons altogether. Velocity-selective coherent population trapping (VSCPT) and Raman cooling use the first approach.

In this section we discuss a simple model of 1D VSCPT based on a three-level lambda transition. More detailed discussions and the extension to 3D can be

found in the 1990 Les Houches lectures of Cohen-Tannoudji (1992). The 2D VSCPT cooling of metastable He to 250 nK, a factor of 16 below the recoil limit, was reported in 1994 (Lawall *et al.* 1994).

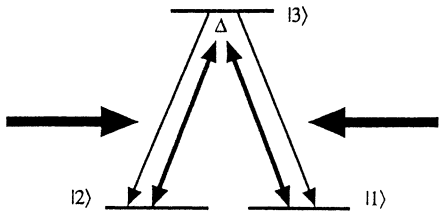

Fig. 5. Schematic diagram of the atomic levels, lasers and transitions used in VSCPT.

We assume that the ground levels are degenerate and that the two counter-propagating lasers have the same frequency, and opposite circular polarisations, see Fig. 5. The interaction picture Hamiltonian is

$$H_{\mathrm{VSCPT}} = \frac{p^2}{2M} - \hbar\Delta|3\rangle\langle 3| + d\mathcal{E}[e^{ikz}|3\rangle\langle 1| + e^{-ikz}|3\rangle\langle 2| + \mathrm{h.c.}]\,, \tag{30}$$

where for simplicity we have assumed that the two transitions have the same dipole moment, d. Note that the plane-wave spatial dependence of the mode in the direction of propagation z has been made explicit. A set of states closed under this Hamiltonian is $\{|\mathrm{NC}, p\rangle, |\mathrm{C}, p\rangle, |3, p\rangle\}$. The first two states are defined by

$$|\mathrm{NC}, p\rangle \equiv \sqrt{\tfrac{1}{2}}(|1, p - \hbar k\rangle - |2, p + \hbar k\rangle)\,, \tag{31}$$

$$|\mathrm{C}, p\rangle \equiv \sqrt{\tfrac{1}{2}}(|1, p - \hbar k\rangle + |2, p + \hbar k\rangle)\,. \tag{32}$$

The 'NC' stands for non-coupling and the 'C' for coupling. The interesting thing is the action of the Hamiltonian equation (32) on $|\mathrm{NC}, p\rangle$. Since $\exp(ikz)$ generates a momentum-space displacement of the momentum eigenstate $|p\rangle$ to $|p + \hbar k\rangle$, then

$$\begin{aligned} H_{\mathrm{VSCPT}}|\mathrm{NC}, p\rangle &= \sqrt{\tfrac{1}{2}}\left\{\frac{(p - \hbar k)^2}{2M}|1, p - \hbar k\rangle - \frac{(p + \hbar k)^2}{2M}|2, p + \hbar k\rangle\right\} \\ &= \left\{\frac{p^2}{2M} + \frac{(\hbar k)^2}{2M}\right\}|\mathrm{NC}, p\rangle - \frac{\hbar k p}{M}|\mathrm{C}, p\rangle\,. \end{aligned} \tag{33}$$

For $p = 0$ $|\mathrm{NC}, p\rangle$ is an eigenstate of the kinetic energy and has no coupling to any other state. This is called a dark state because it does not interact with the field. VSCPT works by accumulating atoms in the non-coupling states $|\mathrm{NC}, p \approx 0\rangle$. The non-coupling states are populated via momentum diffusion due to spontaneous emission from the excited state. The coupling amplitude out of them into $|\mathrm{C}, p\rangle$ states is proportional to p and hence their lifetime increases as their momentum p decreases.

In principle there is no minimum temperature for VSCPT. The range of populated non-coupling states near $p = 0$ decreases with time as they are pumped out via the coupling state. This is because the momentum diffusion into a particular momentum group is independent of its momentum, while the $|\mathrm{NC}, p\rangle \leftrightarrow |\mathrm{C}, p\rangle$ coupling amplitude is proportional to p, and hence vanishes as $p \to 0$.

The dark state $|\mathrm{NC}, p = 0\rangle$ is a quantum mechanical superposition of the atom moving to the left and to the right with the recoil momentum $\hbar k$. In the 2D case the corresponding dark state is a superposition of four atomic momentum states. These states were observed in a Paris experiment (Lawall *et al.* 1994). To confirm the superposition, rather than an incoherent mixture, would require interferometry, which remains to be done.

(2f) Raman Cooling

Like VSCPT, Raman cooling works by isolating the atoms near zero velocity from the cooling fields. However, there is no dark state in Raman cooling; rather the extremely narrow linewidths possible for Raman transitions enable tuning of the Raman pulses so that they do not affect the zero-velocity group.

Because the energy difference between the levels in a Raman transition can be very small, they can have narrow linewidths. This can be used to select correspondingly narrow velocity groups, and push them around. Kasevich and Chu (1992) used this method to push atoms towards zero velocity and achieved 100 nK for Na in 1D, which is 10 times below recoil. In 2D and 3D they did not quite get to recoil although they beat polarisation gradient cooling by a factor of nearly 20 (Davidson *et al.* 1994).

Raman cooling uses a sequence of Raman pulses from counter-propagating lasers to push atoms towards zero velocity. Each Raman transition changes the atomic velocity by $2\hbar k$. The pulses are designed so that zero-velocity atoms are unaffected, and the accuracy with which this can be achieved is one of the limits to the cooling. Since many Raman cycles are needed for cooling, the atoms must be repumped to their original state. The zero-velocity state is populated randomly by atoms which have zero velocity after repumping.

(2g) Evaporative Cooling

Evaporative cooling has achieved the lowest 3D temperatures to date, 170 nK for Rb (Anderson *et al.* 1995), and 100 nK for Li (Bradley *et al.* 1995). These temperatures should be compared to the recoil limit temperatures, equation (18), of $T_{\mathrm{recoil}} = 230$ nK for Rb and $T_{\mathrm{recoil}} = 5{\cdot}5\ \mu$K for Li. This is what made Bose–Einstein condensation of these atoms possible. The cooling is achieved by bleeding off the highest-energy atoms from the trap. Thermalisation of the remaining atoms by elastic collisions produces cooling. After a subsequent adiabatic expansion, Anderson *et al.* (1995) reported a temperature of 20 nK.

The trap is magnetic, see Section 3*d*, so that no optical heating occurs. Only atoms in magnetic states such that their magnetic dipole is attracted to the trap centre are trapped. If the magnetic state is changed the atoms are no longer trapped and they escape. Such spin flips are induced by RF fields tuned to a Zeeman splitting frequency. Since this frequency depends on the local magnetic field strength, spin flips can be selectively induced in the outer parts of the traps.

These are precisely the regions occupied by the high-energy atoms. Progressive cooling is achieved by ramping down the RF frequency. This moves the resonance region towards the centre of the trap, where fields are lowest, and allows colder atoms to evaporate.

3. Trapping

The optical Earnshaw theorem states that atoms for which the dissipative force (see Section 1*b*), is proportional to the intensity cannot be trapped by static configurations of laser beams (Ashkin and Gordon 1983). It is true for the same reason that the classical Earnshaw theorem is true, see Section 3*c*. In a region of space without sources or sinks for light there is as much energy flowing in as out, and the dissipative force is in the same direction as the energy flow.

Fortunately the conditions of the theorem can be violated by adding external fields (Pritchard *et al.* 1986). In the case of the highly successful magneto-optical trap this is an inhomogeneous magnetic field which Zeeman-shifts the transition so that the force is not just proportional to the local intensity.

(3a) Optical Molasses

Optical molasses, discussed in Section 2*a*, does not trap atoms. However, because the atomic motion is diffusive rather than ballistic, the atoms can take seconds to travel centimetres (Chu *et al.* 1985). The dynamics is that of Einstein–Langevin Brownian motion (Gardiner 1985). Using the damping constant of equation (22),

$$\alpha \equiv \hbar k \gamma s_0 \frac{2\Delta k}{\Delta^2 + \gamma^2/4}\,, \tag{34}$$

we have the Langevin equation for the 1D position x of a Doppler-cooled atom,

$$M\frac{\mathrm{d}^2 x}{\mathrm{d}t^2} = \alpha v + N\,, \tag{35}$$

where we have introduced the zero mean noise term N. An equation for $\langle x^2 \rangle$ may be found after multiplying equation (35) by x and using $\langle Mv^2/2 \rangle = k_\mathrm{B}T/2$,

$$\frac{\mathrm{d}\langle x^2 \rangle}{\mathrm{d}t} = \frac{2k_\mathrm{B}T}{\alpha} + C\exp(-\alpha t/M)\,, \tag{36}$$

where C is an integration constant. For long times the exponential on the right-hand side can be ignored and then

$$\langle x^2 \rangle - \langle x_0^2 \rangle = \frac{2k_\mathrm{B}T}{\alpha}t\,. \tag{37}$$

For Na the root mean squared displacement over 1 s is about a few centimetres for $T = 100\ \mu\mathrm{K}$.

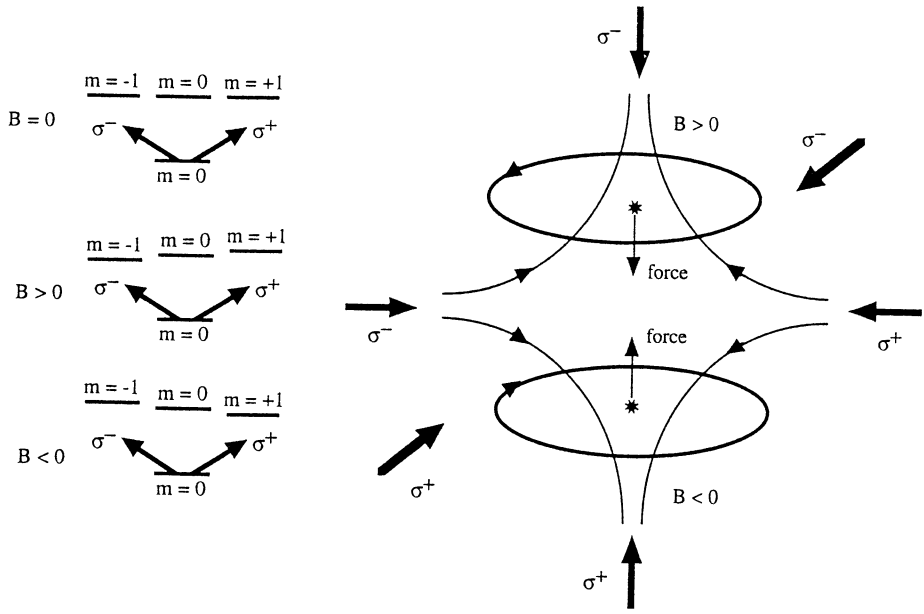

Fig. 6. The magneto-optical trap (MOT). The left part of the diagram schematically shows Zeeman-shifting of a $J = 0 \leftrightarrow J = 1$ transition associated with positive and negative magnetic fields. The right part schematically shows the magnetic field and laser configuration in a MOT. The lasers are labelled by their circular polarisation, either σ^+ or σ^-. The resultant net forces on atoms at two locations are shown.

(3b) Magneto-optical Traps (MOTs)

Magneto-optical traps are now quite common (Wieman *et al.* 1995). They are also known as Zeeman-optical traps, or ZOTs. They use an inhomogeneous magnetic field to produce a position-dependent scattering force. The magnetic field Zeeman-shifts transitions towards or away from resonance with red-detuned, counter-propagating, oppositely circularly polarised laser beams. Consider a $J = 0 \leftrightarrow J = 1$ system. The two transitions coupling to circularly polarised light are shifted by positive and negative magnetic fields as shown in Fig. 6. The magnetic field generated by anti-Helmholtz coils is also shown in Fig. 6. For an atom displaced towards the σ^- polarised beam, the magnetic field becomes more positive and it Zeeman-shifts the σ^- transition into resonance and the σ^+ transition away from resonance. Hence the scattering from the σ^- beam dominates and the atom is pushed back towards the centre of the trap. The magnetic field and laser polarisations are such that atoms are pushed back to the centre after displacement in any direction.

The MOT lasers cool the atoms too. An atom stopping at its turning point is accelerated back towards the centre. However, once the Doppler shift kv exceeds the linewidth γ, it is no longer accelerated. Hence the maximum rebound speed is about γ/k, corresponding to a temperature of about $M(\gamma/k)^2/k_B$ (Metcalf and van der Straten 1994). This is much higher than the Doppler limit, equation (27).

(3c) Ion Traps

Ion traps have certain advantages over optical traps (Blatt 1992). Most importantly, the trapping does not rely on interaction with light. The potentially extremely small dissipation in ion traps has allowed the demonstration of quantum logic gates (Monroe *et al.* 1995). They are one of the more promising ways of realising quantum computers (Cirac and Zoller 1995).

Since the divergence of the electric field in free space is zero, any region must have field lines both going in and coming out. Equivalently, there can be no maxima or minima of the electrostatic potential in free space. This is the content of Earnshaw's electrostatic theorem. Consequently an ion cannot be trapped by electrostatic fields alone. This problem has been solved in two ways: by adding a magnetic field, the Penning trap, or by oscillating the electric field, the Paul trap. A quadrupole potential

$$V = V_0(r^2 - 2z^2)\,, \tag{38}$$

where r is the radial coordinate, is produced by the ring and endcap electrode configuration shown in Fig. 7.

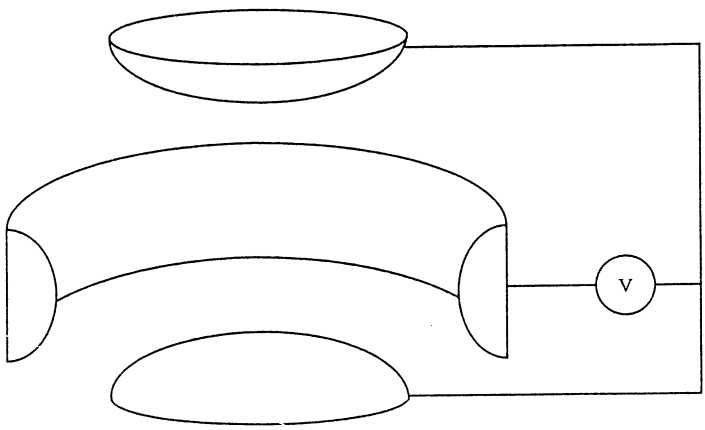

Fig. 7. Ion trap electrodes. Only half the ring electrode is shown. The z direction is vertical and the radial direction is horizontal.

The Penning trap achieves radial confinement with an axial magnetic field in the z direction. This inhibits radial motion by converting it to circular cyclotron motion about the magnetic field lines. The overall motion of the ion is the combination of a slow magnetron rotation ($\approx$10 kHz) about the z axis and the fast cyclotron motion ($\approx$1000 kHz) about the local magnetic field lines. The electrostatic field provides confinement in the z direction. The axial oscillation frequency lies between these two.

The Paul trap adds RF time dependence to the potential equation (38) of the form $V_0 = V_{\mathrm{DC}} + V_{\mathrm{AC}} \cos \omega t$. This allows a dynamic stability. Again the ion motion has two components: slow, approximately harmonic motion in the axial and radial directions, and rapid micromotion oscillation about the local position at the driving frequency ($\approx$10 MHz).

(3d) Magnetic Traps

Magnetic traps confine atoms by exerting a force on the atomic magnetic dipole moment. Many different trap configurations have been proposed (Bergeman *et al.* 1987). Since they avoid laser heating, and the Coulomb repulsion of ions, magnetic traps have been used to Bose–Einstein condense atoms.

The force is the gradient of the dipole energy $-\boldsymbol{\mu}.\boldsymbol{B}$, where $\boldsymbol{\mu}$ is the dipole moment of the magnetic sub-level of the atom and $\boldsymbol{B}$ is the magnetic field. For sufficiently slow atomic motion the magnetic sub-level adiabatically follows the changing direction of the magnetic field as it moves around the trap. For example, an atom in the local ground state remains in the local ground state. Consequently its magnetic moment changes. Atoms in magnetic sub-levels whose Zeeman energy $-\boldsymbol{\mu}.\boldsymbol{B}$ decreases with magnetic field strength are forced towards the field minimum.

Anderson *et al.* (1995) used a variation on the simple quadrupole trap formed with anti-Helmholtz coils (Midgall *et al.* 1985), called the time-averaged orbiting potential, or TOP, trap. This overcomes a problem with the simple quadrupole trap caused by its minimum being zero magnetic field. Close to $B = 0$ the Zeeman levels are nearly degenerate and the atomic state may no longer adiabatically follow the magnetic field. Non-adiabatic transitions to non-trapped magnetic sublevels can occur, leading to trap loss.

This problem is particularly bad in quadrupole traps because the field increases linearly in all directions away from the minimum, so the field derivative is not zero at zero field. The TOP trap adds an RF field which rotates the field zero in a circle. The time-averaged field then has a non-zero, quadratic minimum where the zero previously was. Atoms are still lost from the instantaneous zero, but they are high-energy atoms with respect to the time-averaged potential and hence contribute to evaporative cooling.

Bradley *et al.* (1995) used an arrangement of six permanent magnets to produce a field with a non-zero minimum in which they reported Bose–Einstein condensation of Li.

(3e) Gravitational Traps

Gravity is an important consideration for cold atoms. The energy gained by a Na atom falling through 1 mm is about 4×10^{-28} J, or more than twenty times the recoil energy. Gravity can be used to trap atoms in a trampoline configuration. Ten bounces of about 3 mm height have been observed experimentally off a parabolic evanescent wave reflector (Aminoff *et al.* 1993). This corresponds to a trapping time of about 0·1 s. This result can probably be substantially improved by enhancing the evanescent field. Confinement times at least 50 times longer have been obtained using two sheets of blue-detuned light to form a 'V' in which atoms bounce (Davidson *et al.* 1995).

Other reflector shapes such as pyramids and cones have been analysed (Söding *et al.* 1995; Dowling and Gea-Banacloche 1995). Recoil-limited Sisyphus cooling mechanisms which utilise gravity can be incorporated. For example, if the sub-level changes during the bounce, the average force on the way out can be less than that on the way in (Ovchinnikov *et al.* 1995), leading to an inelastic, cooling bounce.

Acknowledgments

Thanks to J. Hope for reading the manuscript and suggesting improvements. Thanks to the participants in the Workshop on Atom Optics for providing corrections.

References

Adams, C. S., Sigel, M., and Mlynek, J. (1994*a*). *Phys. Reports* **240**, 1.
Adams, C. S., Carnal, O., and Mlynek, J. (1994*b*). *Adv. At. Mol. Opt. Phys.* **34**, 1.
Allen, L., and Eberly, J. H. (1987). 'Optical Resonance and Two-level Atoms' (Dover: NY).
Allen, L., Beijersbergen, M. W., Spreeuw, R. J. C., and Woerdman J. P. (1992). *Phys. Rev.* A **45**, 8185.
Aminoff, C. G., Steane, A. M., Bouyer, P., Desbiolles, P., Dalibard, J., and Cohen-Tannoudji, C. (1993). *Phys. Rev. Lett.* **71**, 3083.
Anderson, M. H., Ensher, J. R., Matthews, M. R., Wieman, C. E., and Cornell, E. A. (1995). *Science* **269**, 198.
Ashkin, A. (1972). *Sci. Am.*, Feb. p. 63.
Ashkin, A., and Gordon J. P. (1983). *Opt. Lett.* **8**, 511.
Ashkin, A., Dziedzic, J., and Yamane, T. (1987). *Nature* **330**, 769.
Ashkin, A., Schutze, K., Dziedzic, J. M., Euteneuer, U., and Schliwa, M. (1990). *Nature* **348**, 346.
Aspect, A., Dalibard, J., Heidmann, A., Salomon, C., and Cohen-Tannoudji, C. (1986). *Phys. Rev. Lett.* **57**, 1688.
Bergeman, T., Erez, G., and Metcalf, H. J. (1987). *Phys. Rev.* A **35**, 1535.
Blatt, R. (1992). *In* 'Fundamental Systems in Quantum Optics: Les Houches session LIII' (Eds J. Dalibard, J.-M. Raimond and J. Zinn-Justin), p. 253 (North-Holland: Amsterdam).
Bradley, C. C., Sackett, C. A., Tollett, J. J., and Hulet, R. G. (1995). *Phys. Rev. Lett.* **75**, 1687.
Chu, S. (1991). *Science* **253**, 861.
Chu, S., Hollberg, L., Bjorkholm, J. E., Cable, A., and Ashkin, A. (1985). *Phys. Rev. Lett.* **55**, 48.
Cirac, J. I., and Zoller, P. (1995). *Phys. Rev. Lett.* **74**, 4091.
Cohen-Tannoudji, C. (1992). *In* 'Fundamental Systems in Quantum Optics: Les Houches session LIII' (Eds J. Dalibard, J.-M. Raimond and J. Zinn-Justin), p. 1 (North-Holland: Amsterdam).
Cohen-Tannoudji, C., and Phillips, W. D. (1990). *Phys. Today* **43**, No. 10, 33.
Cohen-Tannoudji, C., Dupont-Roc, J., and Grynberg, G. (1992). 'Atom–Photon Interactions' (Wiley: NY).
Dalibard, J., and Cohen-Tannoudji, C. (1985). *J. Opt. Soc. Am.* B **2**, 1707.
Davidson, N., Lee, H.-J., Kasevich, M., and Chu, S. (1994). *Phys. Rev. Lett.* **69**, 3158.
Davidson, N., Lee, H.-J., Adams, C. S., Kasevich, M., and Chu, S. (1995). *Phys. Rev. Lett.* **74**, 1311.
Dowling, J. P., and Gea-Banacloche, J. (1995), 'Quantum atomic dots', unpublished.
Gardiner, C. W. (1985). 'Handbook of Stochastic Methods', 2nd ed. (Springer: Berlin).
He, H., Friese, M. E., Heckenberg, N. R., and Rubinsztein-Dunlop, H. (1995). *Phys. Rev. Lett.* **75**, 826.
Kasevich, M., and Chu, S. (1992). *Phys. Rev. Lett.* **69**, 1741.
Kastberg, A., Phillips W. D., Rolston, S. L., and Spreeuw R. J. C. (1995). *Phys. Rev. Lett.* **74**, 1542.
Lawall, J., Bardou, F., Saubamea, B., Shimizu, K., Leduc, M., Aspect, A., and Cohen-Tannoudji, C. (1994). *Phys. Rev. Lett.* **73**, 1915.
Lett, P., Watts, R., Westbrook, C., Phillips, W. D., Gould, P., and Metcalf, H. (1988). *Phys. Rev. Lett.* **61**, 169.
Liang, H., Wright, W. H., He, W., and Berns, M. W. (1991), *Exp. Cell Res.* **197**, 21.
Loudon, R. (1973). 'The Quantum Theory of Light', Chap. 4 (Oxford).
Mallove, E. F., and Matloff, G. L. (1989). 'The Starflight Handbook' (Wiley: NY).

Marksteiner, S., Savage, C. M., Zoller, P., and Rolston S. (1994). *Phys. Rev.* A **50**, 2680.
Messiah, A. (1966). 'Quantum Mechanics', Vol. II, chapter XVII (North-Holland: Amsterdam).
Metcalf, H., and van der Straten, P. (1994). *Phys. Reports* **244**, 203.
Midgall, A. L., Prodan, J. V., Phillips, W. D., Bergeman, T. H., and Metcalf, H. J. (1985). *Phys. Rev. Lett.* **54**, 2596.
Miller, J. D., Cline, R. A., and Heinzen, D. J. (1993). *Phys. Rev.* A **47**, 4567.
Minogin, V. G., and Letokhov, V. S. (1987). 'Laser Light Pressure on Atoms' (Gordon and Breach: NY).
Monroe, C., Meekhof, D. M., King, B. E., Itano, W. M., and Wineland, D. J. (1995), 'Demonstration of a universal quantum logic gate', unpublished.
Ovchinnikov, Yu.B., Söding, C. G. and Grimm, R. (1995). *JETP Lett.* **61**, 21.
Pritchard, D., Raab, E. L., Bagnato, V., Wieman, C. E., and Watts, R. N. (1986). *Phys. Rev. Lett.* **57**, 310.
Söding, C. G., Grimm, R., and Ovchinnikov, Yu. B. (1995). *Opt. Commun.* **119**, 652.
Stenholm, S. (1986). *Rev. Mod. Phys.* **58**, 699.
Steubing, R. W., Cheng, S., Wright W. H., and Berns M. W. (1991). *Cytometry* **12**, 505.
Tadir, Y., Wright, W. H., Vafa, O., Liaw, L. H., Asch, R., and Berns, M. W. (1991). *Human Reprod.* **6**, 1011.
Wieman, C. E., Flowers, G., and Gilbert, S. (1995). *Am. J. Phys.* **63**, 317.
Wiseman, H. M, and Collett, M. J. (1995). *Phys. Lett.* A **202**, 246.

Manuscript received 19 October, accepted 17 December 1995